

No. 576

September 2017

**Dual weighted residual error estimation
for the finite cell method**

P. Di Stolfo, A. Rademacher, A. Schröder

ISSN: 2190-1767

Dual weighted residual error estimation for the finite cell method

August 18, 2017

P. Di Stolfo, paolo.distolfo@sbg.ac.at, University of Salzburg, Hellbrunner Straße 34, 5020 Salzburg, Austria

A. Rademacher, andreas.rademacher@tu-dortmund.de, Fakultät für Mathematik (LS X), Technische Universität Dortmund, 44221 Dortmund, Germany

A. Schröder, andreas.schroeder@sbg.ac.at, Department of Mathematics, University of Salzburg, Hellbrunner Straße 34, 5020 Salzburg, Austria

Abstract

The paper presents a goal-oriented error control based on the dual weighted residual method (DWR) for the finite cell method (FCM), which is characterized by an enclosing domain covering the domain of the problem. The error identity derived by the DWR method allows for a combined treatment of the discretization and quadrature error introduced by the FCM. We present an adaptive strategy with the aim to balance these two error contributions. Its performance is demonstrated for some two-dimensional examples.

Keywords: Finite Cell Method, Goal-oriented error estimation, Dual-weighted residual method

Classification: 65N15; 65N85

Acknowledgements. The first and the last author gratefully acknowledge support by the Deutsche Forschungsgemeinschaft in the Priority Programme 1748 “Reliable simulation techniques in solid mechanics. Development of non-standard discretization methods, mechanical and mathematical analysis” under the project “High-order immersed-boundary methods in solid mechanics for structures generated by additive processes”, Grant SCHR 1244/4-1.

1 Introduction

The finite cell method (FCM) is a well-established variant of the general fictitious domain approach [35, 16, 17] and was developed by Parvizian, Düster, and Rank [26, 14]. It has been applied to a vast number of both linear and nonlinear problems, including linear elasticity in 2D and 3D [14], shell problems [30], biomechanical problems [39, 40], wave

propagation [19], elastoplasticity [1], and topology optimization in structural mechanics [25].

The basic idea of the FCM is to replace the possibly complicated domain of the problem by an enclosing domain of a geometrically simple shape, e.g., a (paraxial) quadrilateral in 2D or (paraxial) hexahedron in 3D. As the enclosing domain can be trivially subdivided into (paraxial) quadrilateral or hexahedral cells, mesh generation is simplified substantially. The finite element space is constructed on these cells, from which the name of the method is derived. To recover the geometry of the original problem, the integrals in the variational formulation of the problem are approximated by quadratures defined on the covering mesh of finite cells. To this end, an approximation of the original domain of sufficient quality has to be available, which is typically provided by a separate quadrature mesh. However, this approximation introduces a quadrature error which is assumed to be lower than the discretization error. A first mathematically rigorous investigation of the FCM for exact integration and certain boundary conditions as well as numerical experiments for inexact integration are provided in [11].

While it has become standard for modern finite-element techniques to include a-posteriori error control and adaptivity, error estimators have neither been derived nor applied to the FCM to this date. In this work, we focus on the dual-weighted residual error (DWR) estimation method, which has become one of the most popular a-posteriori techniques for standard finite elements in the last two decades. It is based on the preliminary work by Eriksson et al. [15] and was developed by Becker and Rannacher [5]. The DWR method allows for goal-oriented error estimation and, thus, supports more general, user-defined, possibly nonlinear expressions to be estimated, such as norms, point values, averages, or lift and drag coefficients, see [2] for an overview. The method relies on representing the error in terms of the solution of a dual problem, which is typical as duality arguments are the basis of many techniques in so-called goal-oriented error control [24, 27]. The DWR method has been applied to many practical problems including fluid mechanics, chemically reactive flows, and fluid-structure interaction (see, e.g., [3, 8, 18, 37, 33, 38]), as well as simplified Signorini and (frictional) contact problems, see [36, 7, 29].

A-posteriori error estimates are well-developed with respect to exact discrete solutions, i.e., solutions determined with no computational error incurred by, e.g., iterative methods or inexact integration. However, there are only a few publications dealing with a-posteriori error estimates for inexact discrete solutions determined by an iterative process, such as the multigrid method [4] or Newton's method in the context of nonlinear problems [31]. A common idea of these approaches is to apply a stopping criterion that is based on balancing the discretization error with the iteration error.

In this article, we discuss the derivation and application of the DWR method in the FCM context in order to estimate both the discretization error and the quadrature error with respect to a goal functional, along with an adaptive strategy with the aim to balance these two contributions by either refining the finite-cell mesh or its associated quadrature mesh. We utilize localization strategies for the DWR method by Richter and Wick [34] and Braack and Ern [9] which do not require jumps over element facets and, thus, are well-suited for the FCM.

The outline of the paper is as follows: In Section 2, we give an overview of the FCM. Section 3 discusses the DWR method for goal-oriented a-posteriori error estimation

and provides the error identity containing terms representing the discretization and the quadrature error. An adaptive strategy realizing both discretization and quadrature mesh refinements is discussed in Section 4. In Section 5, numerical experiments for a smooth and a non-smooth 2D example are presented. Finally, conclusions are drawn in Section 6.

2 Abstract framework for the finite cell method

In this section, we present a general nonlinear setting for the finite-cell method (FCM). For this purpose, let $\Omega \subset \mathbb{R}^d$ be a bounded domain and $\hat{\Omega} \supseteq \Omega$ be a paraxial d -dimensional interval (i.e., a rectangle for $d = 2$ or a cuboid for $d = 3$), and let $\Gamma_D \subseteq \partial\Omega$ be the Dirichlet boundary part.

Given a Hilbert space V of functions defined on Ω with its dual space V^* and an operator $A : V \rightarrow V^*$, we aim to find a solution $u \in V$ such that

$$A(u)(\varphi) = 0 \quad \forall \varphi \in V, \quad (1)$$

where we assume that (1) is uniquely solvable. Furthermore, we assume there exists a space \hat{V} of functions defined on $\hat{\Omega}$ extending V , i.e., $\hat{V}|_{\Omega} \supseteq V$. Also, we assume there exists an operator $\hat{A} : \hat{V} \rightarrow \hat{V}^*$ such that

$$A(v)(\varphi) = \hat{A}(v_0)(\varphi_0) \quad \forall v, \varphi \in V,$$

where w_0 denotes the extension by zero onto $\hat{\Omega}$ of a function w defined on Ω .

In the discrete setting, a triangulation \mathcal{T}_h of $\hat{\Omega}$ into intervals and a finite-element space $V_h \subseteq \hat{V}$ on \mathcal{T}_h can be constructed easily due to the simple form of $\hat{\Omega}$. In the framework used in the following, we assume $V_h|_{\Omega} \subseteq V$, i.e., the space of restrictions is conforming. The discrete problem is to find a solution $u_h \in V_h$ such that

$$\hat{A}(u_h)(\varphi_h) = 0 \quad \forall \varphi_h \in V_h. \quad (2)$$

It is assumed that the contributions $\left| \hat{A}(u_h)(\varphi_h) - A(u_h|_{\Omega})(\varphi_h|_{\Omega}) \right|$ are sufficiently small so that the model error can be neglected. To illustrate the spaces and operators, we consider a 2D example based on the Poisson model problem

$$A(u)(\varphi) := \int_{\Omega} \nabla u \cdot \nabla \varphi - \int_{\Omega} f \varphi = 0 \quad \forall \varphi \in V,$$

where $\Omega := (0, 1)^2 \cap B_1(0)$ is the quarter disk, $f \in L_2(\Omega)$, the space $V := H_{\Gamma_D}^1(\Omega) = \{v \in H^1(\Omega); v|_{\Gamma_D} = 0\}$, and $V^* = H_{\Gamma_D}^1(\Omega)^*$ for the Dirichlet part $\Gamma_D := [0, 1] \times \{0\} \subseteq \partial\Omega$. As the operator \hat{A} , we may choose

$$\hat{A}(v)(\varphi) := \int_{\Omega} \nabla v \cdot \nabla \varphi + \epsilon \int_{\hat{\Omega} \setminus \Omega} \nabla v \cdot \nabla \varphi - \int_{\Omega} f \varphi \quad \forall v, \varphi \in \hat{V},$$

where $\hat{\Omega} := (0, 1)^2$, $\epsilon \approx 0$ (e.g., $\epsilon = 10^{-12}$) is a positive parameter large enough to secure coercivity, and

$$\hat{V} := \left\{ v; v \in L_2(\hat{\Omega}), v|_{\Omega} \in V, v|_{\hat{\Omega} \setminus \Omega} \in H^1(\hat{\Omega} \setminus \Omega) \right\}.$$

For the discrete setting, we introduce a triangulation \mathcal{T}_h of $\hat{\Omega}$ consisting of four square elements and define V_h to be the $H^1(\hat{\Omega})$ -conforming finite-element space of degree 1 on \mathcal{T}_h respecting the Dirichlet boundary condition on Γ_D , implying $V_h|_{\Omega} \subseteq V$ and $V_h \subseteq \hat{V}$. Since, here, the boundary of Ω matches a union of facets, Dirichlet boundary conditions can be applied in a strong manner. However, in general, the Dirichlet boundary is non-matching with $\hat{\Omega}$, i.e., it does not equal the union of some facets in $\hat{\mathcal{T}}_h$. In this case, Dirichlet boundary conditions may be applied weakly by, e.g., Nitsche's method [23, 41]. The contributions

$$\left| \hat{A}(v_h)(\varphi_h) - A(v_h|_{\Omega})(\varphi_h|_{\Omega}) \right| = \epsilon \left| \int_{\hat{\Omega} \setminus \Omega} \nabla v_h \cdot \nabla \varphi_h \right|$$

result in a model error of $O(\sqrt{\epsilon})$, see [11, p. 1047].

While the operator \hat{A} is defined on $\hat{\Omega}$, the domains of the involved integrals may depend on Ω . Therefore, for the computation of \hat{A} in the discrete setting, numerical integration has to be performed. In the context of the FCM, this usually involves an approximation of Ω by geometrically simple objects. These approximations result in approximate operators $\hat{A}^{(n)}$ and perturbed discrete problems

$$\hat{A}^{(n)}\left(u_h^{(n)}\right)(\varphi_h) = 0 \quad \forall \varphi_h \in V_h, \quad (3)$$

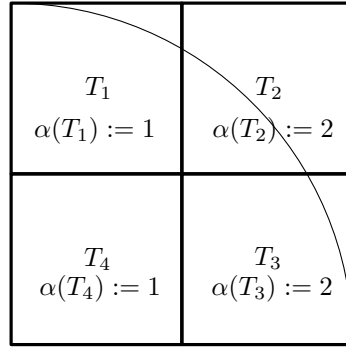
yielding perturbed discrete solutions $u_h^{(n)} \in V_h$. A geometrically simple replacement for Ω used in practice is the spacetree with its specializations to two and three dimensions commonly referred to as quadtree and octree, respectively [12]. Here, to each element $T \in \mathcal{T}_h$, a set of intervals Q_T is assigned via a number $\alpha(T) \in \mathbb{N}_0$ indicating the number of recursive refinements of T towards the boundary $\partial\Omega$. The set Q_T is generated by the following recursive procedure:

1. Set $i := 0$, $Q_T^{(i)} := \{T\}$.
2. If $i = \alpha(T)$, then $Q_T := Q_T^{(i)}$, exit. Otherwise, replace each interval in $Q_T^{(i)}$ that is intersected nontrivially by $\partial\Omega$ by 2^d sub-intervals, yielding $Q_T^{(i+1)}$. Increase i by 1 and go to step (ii).

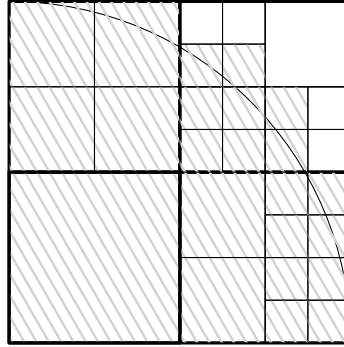
Finally, as an approximation $\Omega^{(n)}$ of the domain of integration Ω , one may use the union of all intervals in any Q_T having non-trivial intersection with Ω . The union of the remaining intervals is then an approximation to $\hat{\Omega} \setminus \Omega$. Similarly, an approximation to $\hat{\Omega}$ can be obtained. For the approximation of the integrals involved in the operators $\hat{A}^{(n)}$, the usual quadrature rules used in the finite-element context are applied on each interval.

The result of the procedure is visualized in Figure 1 for a finite-cell mesh for the quarter disk, where the unit square is subdivided into four equally sized elements, along with the assigned number of recursive refinements.

The presented procedure for establishing the space-tree only makes use of a point-in-domain test, which is typically applied to sample points of each interval (e.g., the four vertices of a rectangle). Thus, the condition whether an interval intersects $\partial\Omega$ nontrivially is checked only approximately. Due to its simplicity, the space-tree can be easily applied to complicated geometries. An obvious disadvantage is the fact that it offers only a piecewise constant approximation to $\partial\Omega$. Therefore, a high number of recursive refinements



(a) A finite-cell discretization of the unit square $\hat{\Omega}$ covering the quarter disk Ω .



(b) The resulting quadtree. A possible approximation to Ω is shaded.

Figure 1: Visualization of the quadtree

may be required to approximate the domain sufficiently well. For domains with smooth boundaries, higher-order approximations may be used. In the context of the FCM, several improvements over the space-tree have been developed, see, e.g., [21, 22, 20].

3 The dual weighted residual method

In this section, we tailor the dual weighted residual (DWR) method for a (possibly nonlinear) problem and a (possibly nonlinear) goal functional to the FCM setting. To this end, we consider the spaces and operators introduced in Section 2 and, in addition, assume A to be three times Gateaux-differentiable. Moreover, let $J : V \rightarrow \mathbb{R}$ be a three times Gateaux-differentiable goal functional. For the k th order Gateaux derivative of a function $g : X \rightarrow Y$ for Banach spaces X, Y in a point $x \in X$, we adopt the usual identification $g^{(k)}(x)(\psi_1, \dots, \psi_k) = g^{(k)}(x)(\psi_1) \cdots (\psi_k)$, indicating that $g^{(k)}(x)$ is k -linear.

For the unique solution $u \in V$ of the problem in eq. (1), we may formulate the following trivial optimization problem which connects the problem with the goal functional:

$$u = \arg \min_{\varphi \in V} J(\varphi) \quad \text{subject to} \quad A(u)(\varphi) = 0 \quad \forall \varphi \in V.$$

Introducing the Lagrangian $\mathcal{L} : V \times V \rightarrow \mathbb{R}$ with $\mathcal{L}(v, w) := J(v) - A(v)(w)$, we seek a

Lagrangian multiplier $z \in V$ such that (u, z) is a stationary point of \mathcal{L} , yielding

$$\mathcal{L}'(u, z)(\varphi, \psi) = (J'(u)(\varphi) - A'(u)(\varphi, z), -A(u)(\psi)) = 0 \quad \forall \varphi, \psi \in V.$$

Thus, in addition to seeking a solution u in eq. (1), we seek a function z that solves the dual problem

$$A'(u)(\varphi, z) = J'(u)(\varphi) \quad \forall \varphi \in V. \quad (4)$$

In the FCM setting, the nonconformity $V_h \not\subseteq V$ and the approximation of operators and functionals have to be taken into account in the computation of the discrete solutions. Similar to the case of A and $\hat{A}^{(n)}$ described in Section 2, we assume that approximations $J^{(n)}, J'^{(n)}$ for J, J' exist, where all integrals on Ω occurring in the definition are replaced by a quadrature rule on $\Omega^{(n)}$. Instead of the discrete dual problem, its perturbation

$$\hat{A}'^{(n)}\left(u_h^{(n)}\right)\left(\varphi_h, z_h^{(n)}\right) = J'^{(n)}\left(u_h^{(n)}|_{\Omega}\right)\left(\varphi_h|_{\Omega}\right) \quad \forall \varphi_h \in V_h \quad (5)$$

is solved. We are interested in a representation of the exact error

$$\text{err}_{\text{ex}} := J(u) - J\left(u_h^{(n)}|_{\Omega}\right)$$

which ought to be computable except for minor perturbations: We assume that there exists a sufficiently precise approximation $J^{(n+k)}$ of J for a fixed $k \in \mathbb{N}$, such that the resulting perturbation error is negligibly small. Moreover, the representation should allow for a separation of two error sources, i.e., the discretization and the quadrature. We derive such a representation by adapting the proof stated for the standard FEM case in [31, Prop. 3.1], where a representation of the error with respect to any perturbation $v_h \in V_h$ of the discrete solution is provided. In the FCM setting, we show that the error is composed of the sum of a discretization-related error term, a quadrature-related error term, and some terms which are assumed to be negligibly small (e.g., of higher order). The representation requires computable replacements u^+, z^+ for the unknown solutions u, z , as well as improvements $G^{(n+k)}$ of the approximations $G^{(n)}$ for each $G \in \{A, A', \hat{A}, \hat{A}', J, J'\}$ with the property that $|G^{(n+k)}(\cdot) - G(\cdot)|$ is negligibly small, see below.

Proposition 1. *Let u resp. z be the solution of the primal resp. dual problem in eq. (1) resp. (4) with approximations $u^+, z^+ \in V^+$, where $\hat{V} \supseteq V^+ \supseteq V_h$. Then, for the perturbed discrete solutions $u_h^{(n)}$ resp. $z_h^{(n)}$ of eq. (3) resp. (5), it holds that*

$$\begin{aligned} J(u) - J^{(n+k)}\left(u_h^{(n)}|_{\Omega}\right) &= e_D^{(n+k)}(u^+|_{\Omega}, z^+|_{\Omega}) + e_Q^{(n+k)} \\ &\quad + e_{HO,Q} + e_{HO,J} + e_{HO,\mathcal{L}^+} \\ &\quad + e_{HO,D}(u^+|_{\Omega}, z^+|_{\Omega}) + \mathcal{R}_h^{(3)}, \end{aligned} \quad (6)$$

where

$$\begin{aligned} e_D^{(n+k)}(v, w) &:= \frac{1}{2} \left(\rho\left(w_0 - z_h^{(n)}\right) + \rho^*\left(v_0 - u_h^{(n)}\right) \right), \quad v, w \in V, \\ e_Q^{(n+k)} &:= -\hat{A}^{(n+k)}\left(u_h^{(n)}\right)\left(z_h^{(n)}\right), \end{aligned} \quad (7)$$

$$\begin{aligned}
e_{HO,Q} &:= \hat{A}^{(n+k)}\left(u_h^{(n)}\right)\left(z_h^{(n)}\right) - A\left(u_h^{(n)}|\Omega\right)\left(z_h^{(n)}|\Omega\right), \\
e_{HO,J} &:= \left(J - J^{(n+k)}\right)\left(u_h^{(n)}|\Omega\right), \\
e_{HO,\mathcal{L}} &:= \frac{1}{2}\left(J'\left(u_h^{(n)}|\Omega\right)(e) - J'^{(n+k)}\left(u_h^{(n)}|\Omega\right)(e)\right. \\
&\quad \left.- \left(A'\left(u_h^{(n)}|\Omega\right)\left(e, z_h^{(n)}|\Omega\right) - \hat{A}'^{(n+k)}\left(u_h^{(n)}\right)\left(e_0, z_h^{(n)}\right)\right)\right. \\
&\quad \left.- \left(A\left(u_h^{(n)}|\Omega\right)(e^*) - \hat{A}^{(n+k)}\left(u_h^{(n)}\right)\left((e^*)_0\right)\right)\right), \\
e_{HO,D}(v, w) &:= -e_D^{(n+k)}(v, w) - e_D^{(n+k)}(v, w) \\
&\quad - e_D^{(n+k)}(v - u, w - z), \quad v, w \in V
\end{aligned} \tag{8}$$

for $e := u - u_h^{(n)}|_\Omega$, $e^* := z - z_h^{(n)}|_\Omega$. The residuals ρ, ρ^* are defined as

$$\begin{aligned}
\rho(\cdot) &:= -\hat{A}^{(n+k)}\left(u_h^{(n)}\right)(\cdot), \\
\rho^*(\cdot) &:= J'^{(n+k)}\left(u_h^{(n)}|\Omega\right)(\cdot|_\Omega) - \hat{A}'^{(n+k)}\left(u_h^{(n)}\right)\left(\cdot, z_h^{(n)}\right).
\end{aligned}$$

The higher-order remainder $\mathcal{R}_h^{(3)}$ is given by

$$\begin{aligned}
\mathcal{R}_h^{(3)} &:= \int_0^1 \left(J'''(u_h^{(n)}|\Omega + te)(e, e, e) - A'''(u_h|_\Omega + te)(e, e, e, z_h^{(n)}|_\Omega + te^*) \right. \\
&\quad \left. - 3A''(u_h^{(n)}|_\Omega + te)(e, e, e^*) \right) t(t-1) dt.
\end{aligned}$$

PROOF. Let $\ell : \mathbb{R} \rightarrow \mathbb{R}$ be defined as

$$\ell(t) := \mathcal{L}(\gamma_u(t), \gamma_z(t)) = \mathcal{L}\left(\left(u_h^{(n)}|_\Omega, z_h^{(n)}|_\Omega\right) + t(e, e^*)\right),$$

where $\gamma_u(t) := u_h^{(n)}|_\Omega + te$, $\gamma_z(t) := z_h^{(n)}|_\Omega + te^*$. Note that $\gamma'_u(t) = e$, $\gamma'_z(t) = e^*$. The derivative of ℓ is

$$\ell'(t) = \mathcal{L}'(\gamma_u(t), \gamma_z(t))(e, e^*) \cdot (1, 1)^\top.$$

Applying the definition of \mathcal{L} , we get

$$\ell'(t) = J'(\gamma_u(t))(e) - A'(\gamma_u(t))(e, \gamma_z(t)) - A(\gamma_u(t))(e^*).$$

Applying differentiation twice more yields

$$\ell'''(t) = J'''(\gamma_u(t))(e, e, e) - A'''(\gamma_u(t))(e, e, e, \gamma_z(t)) - 3A''(\gamma_u(t))(e, e, e^*). \tag{9}$$

The error using the exact functional J can be written in the following form:

$$\begin{aligned}
J(u) - J\left(u_h^{(n)}|\Omega\right) &= \mathcal{L}(u, z) + A(u)(z) - \mathcal{L}\left(u_h^{(n)}|_\Omega, z_h^{(n)}|_\Omega\right) - A\left(u_h^{(n)}|\Omega\right)\left(z_h^{(n)}|_\Omega\right) \\
&= \mathcal{L}(u, z) - \mathcal{L}\left(u_h^{(n)}|_\Omega, z_h^{(n)}|_\Omega\right) - A\left(u_h^{(n)}|\Omega\right)\left(z_h^{(n)}|_\Omega\right) \\
&= \ell(1) - \ell(0) - A\left(u_h^{(n)}|\Omega\right)\left(z_h^{(n)}|_\Omega\right) \\
&= \int_0^1 \ell'(t) dt - A\left(u_h^{(n)}|\Omega\right)\left(z_h^{(n)}|_\Omega\right).
\end{aligned}$$

It follows that

$$J(u) - J^{(n+k)}\left(u_h^{(n)}|_\Omega\right) = \int_0^1 \ell'(t) dt + e_Q + e_{HO,Q} + e_{HO,J}.$$

We use the error representation of the trapezoidal rule to obtain

$$\int_0^1 \ell'(t) dt = \frac{1}{2}(\ell'(0) + \ell'(1)) + \frac{1}{2} \int_0^1 \ell'''(t)t(t-1) dt.$$

Since $\ell'''(t)$ has been determined in (9), it remains to inspect the terms $\ell'(0)$ and $\ell'(1)$. We use that $\gamma_u(0) = u_h^{(n)}|_\Omega$, $\gamma_z(0) = z_h^{(n)}|_\Omega$, and $\gamma_u(1) = u$, $\gamma_z(1) = z$, so that

$$\ell'(1) = J'(u)(e) - A'(u)(e, z) - A(u)(e^*) = 0$$

since (u, z) is a stationary point of \mathcal{L} . We see that

$$\begin{aligned} \ell'(0) &= J'\left(u_h^{(n)}|_\Omega\right)(e) - A'\left(u_h^{(n)}|_\Omega\right)\left(e, z_h^{(n)}|_\Omega\right) - A\left(u_h^{(n)}|_\Omega\right)(e^*) \\ &= \rho^*(e_0) + \rho((e^*)_0) + 2e_{HO,\mathcal{L}}. \end{aligned}$$

Thus, $\ell'(0) = 2e_D^{(n+k)}(u, z) + 2e_{HO,\mathcal{L}}$. The definition $\mathcal{R}_h^{(3)} = \frac{1}{2} \int_0^1 \ell'''(t)t(t-1) dt$ and the calculation

$$\begin{aligned} e_D^{(n+k)}(u, z) &= e_D^{(n+k)}(u^+|_\Omega, z^+|_\Omega) - e_D^{(n+k)}(u^+|_\Omega, z) - e_D^{(n+k)}(u, z^+|_\Omega) \\ &\quad - e_D^{(n+k)}(u^+|_\Omega - u, z^+|_\Omega - z) \\ &= e_D^{(n+k)}(u^+|_\Omega, z^+|_\Omega) + e_{HO,D}(u^+|_\Omega, z^+|_\Omega) \end{aligned}$$

imply the proposed error identity. ■

In the finite-cell method, the approximations with index $n+k$ may be obtained from approximations with index n by globally refining the spacetree k times. For sufficiently large k , we may therefore assume that the terms in Eq. (8) are indeed negligibly small compared to the terms $e_D^{(n+k)}(u^+|_\Omega, z^+|_\Omega)$ and $e_Q^{(n+k)}$ from Eq. (7).

To see that $e_Q^{(n+k)}$ can be regarded as a quadrature error term, assume that exact integration is available, i.e., $\hat{A}^{(n+k)} = \hat{A}$, and we may abbreviate $u_h := u_h^{(n)}$, $z_h := z_h^{(n)}$, and $e_Q := e_Q^{(n+k)} = -\hat{A}(u_h)(z_h) = 0$. Inserting the exact solutions u, z , the error representation reduces to

$$J(u) - J(u_h|_\Omega) = e_D(u, z) + \mathcal{R}_h^{(3)} + O(\epsilon)$$

under the assumption that the contribution

$$\begin{aligned} &\left| \hat{A}(u_h)(z_h) - A(u_h|_\Omega)(z_h|_\Omega) \right| + \left| A'(u_h|_\Omega)(e, z_h|_\Omega) - \hat{A}'(u_h)(e_0, z_h) \right| \\ &\quad + \left| A(u_h|_\Omega)(e^*) - \hat{A}(u_h)((e^*)_0) \right| = O(\epsilon), \end{aligned}$$

which is typical for the FCM. Therefore, the term $e_Q^{(n+k)}$ vanishes if all operators are exact. Also, the only remaining term which is not negligibly small is $e_D(u, z)$, which thus

represents the discretization error. If only approximations to the operators are available or a perturbed solution is inserted, the term $e_Q^{(n+k)}$ will be nonzero in general and, thus, may be regarded as a perturbation error. This error may be caused by, e.g., numerical quadrature or by an iterative method as in [31]. Thus, the error representation in eq. (6) allows for a meaningful separation of error sources.

Summarizing, we obtain the approximate error representation

$$\begin{aligned} \text{err}_{\text{ex}} &\approx \text{comp}^{(n+k)} := J(u) - J^{(n+k)}\left(u_h^{(n)}|_\Omega\right) \\ &\approx e_D^{(n+k)}(u^+|_\Omega, z^+|_\Omega) + e_Q^{(n+k)} =: \eta^{(n+k)} \end{aligned} \quad (10)$$

where the terms assumed to be of higher order are neglected. The effectivity index (or overestimation index) is defined as

$$\text{eff}^{(n+k)} := \frac{|\eta^{(n+k)}|}{|\text{comp}^{(n+k)}|}, \quad (11)$$

The question of how to compute the approximations u^+ , z^+ is addressed in Section 3.1. Also, localization techniques for the discretization error are discussed. Finally, the special case of linear problems is addressed in Section 3.2.

3.1 Approximation of the solutions of the continuous problems and localization

The unknown quantities u and z are approximated by computable functions u^+ and z^+ . To this end, several methods have been proposed in the literature. The first method computes approximations by solving the discrete problems in a finite-element space of higher polynomial degree, e.g., by doubling each local polynomial degree [6]. However, this is too expensive except for simple test problems. Usually, patched meshes are employed, i.e., for an element of \mathcal{T}_h with its parent element P in the mesh refinement history, all 2^d children of P are elements of \mathcal{T}_h . This implies that whenever an element is refined, all its siblings are refined as well. In this case, the patches of the mesh can be joined to form a finite-element space $V_{2h,2p}$ of double mesh width and double polynomial degree. The computation of u^+ , z^+ is then approximately as expensive as the computation of $u_h^{(n)}$, $z_h^{(n)}$.

Another method requiring patched meshes uses local higher-order interpolation to compute more accurate approximations by, again, viewing each patch as a single element of a coarser mesh and doubling the polynomial degree [2]. This eliminates the need of computing additional discrete solutions. Under certain regularity assumptions, it can be shown that the error incurred is of higher order, see [2, Section 5.2]. However, one has to take care that the resulting functions are elements of V by ensuring continuity of the interpolation on the boundary of the patches, which is difficult when hanging nodes are present [28].

To perform the finite-cell mesh adaptation, the discretization error $e_D^{(n+k)} := e_D^{(n+k)}(u^+|_\Omega, z^+|_\Omega)$ has to be localized to nonnegative elementwise contributions $\eta_{D,T}^{(n+k)}$. To this end, several methods are available, for all of which good effectivity indices have been demonstrated for many practical problems (see, e.g., the references in the introduction). A first method applies elementwise partial integration leading to an inner residual and a boundary residual

involving integrals over the boundary of each element. An obvious disadvantage of this method is the possibly costly computation of strong residuals and jump terms. Also, the strong adjoint residual formulation may not even be available [34]. In the context of the FCM, another disadvantage consists in the necessity of determining intersections between the boundary of the domain and the element boundaries, as these intersections are not required for the application of the FCM. Also, these intersections have to be determined with great precision in order not to introduce additional errors.

A second method is known as the algebraic filtering approach which is based on the variational formulation and has been described by Braack and Ern [9]. The method relies on patched meshes and the associated canonical finite-element spaces $V_{2h,p}$ and $V_{2h,2p}$ formed by treating each patch as an element of degree p and $2p$, respectively. In order to reconstruct higher-order solutions, interpolation and filtering operators are defined, which we briefly describe in the case of meshes without hanging nodes [34]. As the spaces $V_{h,p}$ and $V_{2h,2p}$ have the same numbers of unknowns in the same Lagrange points, one can define an interpolation operator $i^* : V_{h,p} \rightarrow V_{2h,2p}$ by assigning to $v_h \in V_{h,p}$ the element i^*v_h of $V_{2h,2p}$ uniquely determined by the values of v_h in those Lagrange points. The filtering operator is defined by $\pi_{2h} := \text{id} - i_{2h}$ for a finite-element interpolation operator $i_{2h} : V \rightarrow V_{2h,p}$. The name of the method stems from the observation that $\pi_{2h}v_h$ is a strictly local algebraic process acting on the coefficient vector $\mathbf{v} \in \mathbb{R}^N$ of $v_h \in V_{h,p}$, since $\pi_{2h}v_h = v_h - i_{2h}v_h = \sum_{j=1}^N \mathbf{v}_j(\varphi_{h,j} - i_{2h}\varphi_{h,j}) =: \sum_j (\pi_{2h}\mathbf{v})_j \varphi_{h,j}$ for the basis $(\varphi_{h,j})_{j=1}^N$ of $V_{h,p}$, see [34, eq. (40)]. Finally, the localization of $e_D^{(n+k)}$ to nodal contributions is as follows:

$$\begin{aligned}
e_D^{(n+k)} &\approx \sum_{j=1}^N \frac{1}{2} \left(-\hat{A}^{(n+k)} \left(u_h^{(n)} \right) \left((i^* - \text{id})\varphi_{h,j}(\pi_{2h}\mathbf{z})_j \right) \right. \\
&\quad \left. + J'^{(n+k)} \left(u_h^{(n)} |_{\Omega} \right) \left(\left((i^* - \text{id})\varphi_{h,j}(\pi_{2h}\mathbf{u})_j \right) |_{\Omega} \right) \right. \\
&\quad \left. - \hat{A}'^{(n+k)} \left(u_h^{(n)} \right) \left((i^* - \text{id})\varphi_{h,j}(\pi_{2h}\mathbf{u})_j, z_h^{(n)} \right) \right) \\
&=: \sum_{j=1}^N \tilde{\eta}_{D,j}
\end{aligned} \tag{12}$$

The node-wise error contributions $\eta_{D,j}^{(n+k)} := \left| \tilde{\eta}_{D,j}^{(n+k)} \right|$ are then used for the marking step in the adaptive procedure, e.g., by refining all elements touching node j or by explicitly assigning an elementwise indicator $\eta_{D,T}^{(n+k)}$ based on the node-wise contributions and performing the usual elementwise refinement.

A third method which also uses the variational formulation directly has been proposed by Richter and Wick [34], where a partition of unity $(\psi_j)_{j=1}^N$ for the nodes of the finite-

element mesh is inserted into the representation (6):

$$\begin{aligned}
e_D^{(n+k)} &= \sum_{j=1}^N \frac{1}{2} \left(-\hat{A}^{(n+k)}(u_h^{(n)}) \left((z^+ - z_h^{(n)}) \psi_j \right) \right. \\
&\quad \left. + J'^{(n+k)}(u_h^{(n)}|_\Omega) \left(\left((u^+ - u_h^{(n)}) \psi_j \right) |_\Omega \right) \right. \\
&\quad \left. - \hat{A}'^{(n+k)}(u_h^{(n)}) \left((u^+ - u_h^{(n)}) \psi_j, z_h^{(n)} \right) \right) \\
&=: \sum_{j=1}^N \tilde{\eta}_{D,j}
\end{aligned} \tag{13}$$

Again, the absolute values of the nodal contributions are used for the marking step in the adaptive procedure in the same way as explained for the second method.

To measure the quality of the localization, we define the indicator index

$$\text{ind}_D^{(n+k)} := \frac{\sum_{T \in \mathcal{T}_h} \eta_{D,T}^{(n+k)}}{|e_D^{(n+k)}|} \tag{14}$$

similar to [34, eq. (26)] which takes into account the overestimation of the discretization error caused by taking the absolute value of possibly negative local values $\tilde{\eta}_{D,T}^{(n+k)}$.

The value $e_Q^{(n+k)}$ is used to decide whether the quality of the quadrature mesh as a whole is sufficient for performing the finite-cell computation. We observe that the quality of the solution $u_h^{(n)}$ of the discrete problem as an approximation to u_h depends heavily on the quality of the quadrature mesh. In general, utilizing an insufficient quadrature rule on a single cell (e.g., by a crude approximation via a space-tree) may destroy the quality of the solution $u_h^{(n)}$ and, thus, increase both the true and the estimated discretization error dramatically even though only the quadrature error should increase. Thus, the quadrature error localization would have to be very precise. Therefore, we adapt the quadrature mesh only globally and leave the localization of $e_Q^{(n+k)}$ for future work.

3.2 The linear case

As a special case of the presented setting, let us consider the linear model problem

$$A(u)(\varphi) = 0 \quad \forall \varphi \in V$$

with $A(v)(\varphi) = a(v, \varphi) - F(\varphi)$ for a bilinear form $a : V \times V \rightarrow \mathbb{R}$, a linear form $F \in V^*$, and a possibly nonlinear error functional $J : V \rightarrow \mathbb{R}$. The derivative of A simplifies to $A'(u)(\varphi, \psi) = a(\varphi, \psi)$. Then, the dual problem reads

$$a(\varphi, z) = J'(u)(\varphi) \quad \forall \varphi \in V.$$

We refer to the notation of Prop. 1. The contribution $e_D(u^+|_\Omega, z^+|_\Omega)$ reduces to

$$\begin{aligned} 2e_D(u^+|_\Omega, z^+|_\Omega) &= -\hat{A}^{(n+k)}\left(u_h^{(n)}\right)\left(z^+ - z_h^{(n)}\right) + J'^{(n+k)}\left(u_h^{(n)}|_\Omega\right)\left(\left(u^+ - u_h^{(n)}\right)|_\Omega\right) \\ &\quad - \hat{A}'^{(n+k)}\left(u_h^{(n)}\right)\left(u^+ - u_h^{(n)}, z_h^{(n)}\right) \\ &= \hat{F}^{(n+k)}\left(z^+ - z_h^{(n)}\right) - \hat{a}^{(n+k)}\left(u_h^{(n)}, z^+ - z_h^{(n)}\right) \\ &\quad + J'^{(n+k)}\left(u_h^{(n)}|_\Omega\right)\left(\left(u^+ - u_h^{(n)}\right)|_\Omega\right) - \hat{a}^{(n+k)}\left(u^+ - u_h^{(n)}, z_h^{(n)}\right). \end{aligned}$$

If, additionally, J is linear, we have $J'(\cdot)(\varphi) = J(\varphi)$. Furthermore, under the assumption that $V^+ \supseteq V_h$ and that u^+, z^+ solve the discrete problems

$$\begin{aligned} \hat{a}^{(n+k)}(u^+, v^+) &= \hat{F}^{(n+k)}(v^+) \quad \forall v^+ \in V^+, \\ \hat{a}^{(n+k)}(v^+, z^+) &= J^{(n+k)}(v^+|_\Omega) \quad \forall v^+ \in V^+, \end{aligned}$$

we obtain the simplifications

$$\begin{aligned} 2e_D(u^+|_\Omega, z^+|_\Omega) &= \hat{a}^{(n+k)}\left(u^+, z^+ - z_h^{(n)}\right) - \hat{a}^{(n+k)}\left(u_h^{(n)}, z^+ - z_h^{(n)}\right) \\ &\quad + J^{(n+k)}\left(\left(u^+ - u_h^{(n)}\right)|_\Omega\right) - \hat{a}^{(n+k)}\left(u^+ - u_h^{(n)}, z_h^{(n)}\right) \\ &= \hat{a}^{(n+k)}\left(u^+ - u_h^{(n)}, z^+ - z_h^{(n)}\right) + \hat{a}^{(n+k)}\left(u^+ - u_h^{(n)}, z^+\right) \\ &\quad - \hat{a}^{(n+k)}\left(u^+ - u_h^{(n)}, z_h^{(n)}\right) \\ &= 2\hat{a}^{(n+k)}\left(u^+ - u_h, z^+ - z_h\right). \end{aligned}$$

For the quadrature error contribution, we obtain

$$e_Q^{(n+k)} = \hat{a}^{(n+k)}\left(u_h^{(n)}, z_h^{(n)}\right) - \hat{F}^{(n+k)}\left(z_h^{(n)}\right).$$

Assuming that u_h is the solution of the discrete problem with exact integration, i.e., $\hat{a}(u_h, \varphi_h) = \hat{F}(\varphi_h) \quad \forall \varphi_h \in V_h$, we see that, by adding zero twice,

$$\begin{aligned} e_Q^{(n+k)} &= \left(\hat{a}^{(n+k)}\left(u_h^{(n)}, z_h^{(n)}\right) - \hat{a}\left(u_h, z_h^{(n)}\right)\right) - \left(\hat{F}^{(n+k)}\left(z_h^{(n)}\right) - \hat{F}\left(z_h^{(n)}\right)\right) \\ &= \left(\hat{a}^{(n+k)}\left(u_h^{(n)} - u_h, z_h^{(n)}\right) - (\hat{a} - \hat{a}^{(n+k)})\left(u_h, z_h^{(n)}\right)\right) \\ &\quad - \left(\hat{F}^{(n+k)}\left(z_h^{(n)}\right) - \hat{F}\left(z_h^{(n)}\right)\right). \end{aligned}$$

This shows that the term $e_Q^{(n+k)}$ can be used to measure the error incurred by perturbation of the exact operators.

4 Refinement strategy

As identity (6) allows for a separation of the error into a term representing the discretization error $e_D^{(n+k)}$ and a term representing the quadrature error $e_Q^{(n+k)}$, we may use these

two terms to perform mesh adaptation in order to balance the discretization error and the quadrature error. A similar strategy in [31] balances the discretization and the iteration error that occurs when, e.g., Newton’s method is applied for solving a nonlinear problem.

In the case of finite elements with exact quadrature, each step in the Solve–Estimate–Mark–Refine (SEMR) loop for adaptivity is well-examined at least for linear problems [13, 10]. However, for the finite-cell method, there are no strategies available for choosing the accuracy of the quadrature mesh. In practice, when the spacetime is used, a fixed number of recursive refinements throughout the computation is chosen. However, the chosen depth might be too high and a coarser integration mesh might be sufficient.

A possible heuristic strategy when the spacetime is utilized is the following: Considering the function $\alpha : \mathcal{T}_h \rightarrow \mathbb{N}_0$ from Section 2 assigning to each finite cell the number of recursive quadrature mesh refinements towards the boundary, we set $\alpha \equiv d$ initially for some small $d \in \mathbb{N}_0$. This produces an initial quadrature mesh that is still coarse. During each iteration of the SEMR loop, it is checked whether the overall precision of the quadrature is sufficient for the current finite-cell computation. If this is not the case, then α is increased by 1 and the computation is repeated. The involved check whether the overall precision of the quadrature is sufficient aims at balancing the two error contributions, the discretization and the quadrature error, in particular, the quadrature mesh is refined if the quadrature error exceeds a certain multiple of the discretization error.

An issue that requires attention is the fact that, whenever an element T of the finite-cell mesh is refined and $\alpha(T) = 0$, the quadrature mesh is refined in T as well, so that the quadrature error might decrease when only a decrease in the discretization error is intended. Hence, if $\alpha(T) > 0$, it is reasonable to set $\alpha(T') := \alpha(T) - 1$ for any child T' of T in order not to introduce an additional improvement of the quadrature mesh where only an improvement in the finite-cell mesh is indicated. Furthermore, it is useful to introduce a lower bound $l \in \mathbb{N}_0$ on α , e.g., $\alpha \geq l := 0$, when derefinements are not supported.

The adaptive strategy is summarized in the following steps. We emphasize that the error terms from (10) as well as the finite-cell mesh and the number of quadrature mesh refinements α now depend on the iteration index i of the SEMR loop. Also, to indicate the dependence of the approximate terms on α when the space-tree is used, we replace the generic number n indicating a sequence of approximations to the exact operators and functionals by the number of quadrature mesh refinements per element, given by the function α . Hence, we write $\alpha + k$ instead of $n + k$ indicating that the quadrature mesh defined by α is refined k times globally.

1. Set $i := 0$. Initialize the finite-cell mesh \mathcal{T}_i . Set the number of recursive quadrature refinements per element $\alpha_i \equiv d$ for some initial depth d . Set l to be the minimum possible depth. Choose a stopping criterion, e.g., stop if the maximum number of degrees of freedom is reached or if a prescribed error tolerance is met.
2. Construct the quadrature mesh for \mathcal{T}_i associated to α_i .
3. Solve: Compute solutions $u_{h,i}^{(\alpha_i)}, z_{h,i}^{(\alpha_i)}$ of the perturbed discrete problems from eq. (3), (5). Compute approximations u_i^+, z_i^+ to u, z .
4. Estimate: Choose $k \in \mathbb{N}$ and construct a quadrature mesh on \mathcal{T}_i associated to $\alpha_i + k$ to compute estimators $e_{D,i}^{(\alpha_i+k)}, e_{Q,i}^{(\alpha_i+k)}$ and indicators $\eta_{D,T,i}^{(\alpha_i+k)}$ for each $T \in \mathcal{T}_i$. If the

stopping criterion is fulfilled, stop. If $\left|e_{Q,i}^{(\alpha_i+k)}\right| \geq \rho \left|e_{D,i}^{(\alpha_i+k)}\right|$, set $\alpha_i := \alpha_i + 1$ and go to step 2.

5. Mark: Choose an appropriate marking strategy, such as fixed-fraction marking or maximum marking [5], and mark elements with respect to the local discretization error $\eta_{D,T,i}^{(n+k)}$ for finite-cell mesh refinement.
6. Refine: Refine each marked element in \mathcal{T}_i to obtain \mathcal{T}_{i+1} . For the quadrature mesh, let $\alpha_{i+1} : \mathcal{T}_{i+1} \rightarrow \mathbb{N}_0$ and set $\alpha_{i+1}|_{\mathcal{T}_i \cap \mathcal{T}_{i+1}} := \alpha_i$ except for children T' of any marked element T , where $\alpha_{i+1}(T') := \alpha_i(T) - 1$ unless $\alpha_i(T) - 1 < l$.
7. Increase i by 1 and go to step (ii).

5 Numerical results

We demonstrate the effect of the refinement strategy proposed in Section 4 applied to both linear and nonlinear problems on convex and non-convex circular domains.

5.1 Quarter disk

The first domain is the quarter disk $\Omega := B_1(0) \cap (0, 1)^2$ with Dirichlet boundary part $\Gamma_D := ([0, 1] \times \{0\}) \cup (\{0\} \times [0, 1])$ and Neumann boundary part $\Gamma_N := \partial\Omega \setminus \Gamma_D$. We face the difficulty that the circular domain cannot be represented exactly by quadrilateral finite elements. Thus, we embed Ω into the rectangle $\hat{\Omega} := (0, 1)^2$. The initial finite-cell mesh \mathcal{T}_0 consists of 16 square elements of order 1 and the initial depth of the quadrature mesh is set to $\alpha_0 \equiv 3$. Throughout the computations, $\epsilon = 10^{-12}$ is used.

5.1.1 Linear problem

As a smooth linear model problem, we choose the Poisson problem $-\Delta u = f$, $u|_{\Gamma_D} = 0$, $\partial_n u|_{\Gamma_N} = g_N$. The right-hand side f and the function g_N are such that $u(x, y) := \sin(\pi x) \sin(\pi y)$ is the solution of the Poisson problem. We choose $J(v) := \int_{\Omega} v$ as a goal functional. The corresponding dual problem in weak form is: Find $z \in H_{\Gamma_D}^1(\Omega)$ such that $\int_{\Omega} \nabla z \cdot \nabla \varphi = \int_{\Omega} \varphi$ for all $\varphi \in H_{\Gamma_D}^1(\Omega)$. A high-precision approximation to $J(u)$ may be computed for reference as $J(u) = \int_{\Omega} u \approx 0.3592929181499192$.

For the sake of simplicity of this model problem, the exact solution z is approximated by a higher-order finite-element solution z^+ , for which the same mesh \mathcal{T}_i , but finite elements of order $p = 2$ are used. The error estimates $e_{D,i}^{(\alpha_i+k)}$ and $e_{Q,i}^{(\alpha_i+k)}$ as well as the indicators for the discretization error $\eta_{D,T,i}^{(\alpha_i+k)}$ are computed with $k := 3$. The parameter ρ is set to 0.01.

Figure 2 displays the error terms from Equation (10), i.e., the approximation to the computational error $\text{comp}_i^{(\alpha_i+k)}$, the estimated discretization error $e_{D,i}^{(\alpha_i+k)}$, and the estimated quadrature error $e_{Q,i}^{(\alpha_i+k)}$. Table 1 lists the numerical values corresponding to the finest quadrature mesh used for a given finite-cell mesh. As the effectivity indices (see (11)) are approximately 1.0, we see that the estimation captures the exact error very well. The indicator indices (see (14)) are very similar, which demonstrates that neither

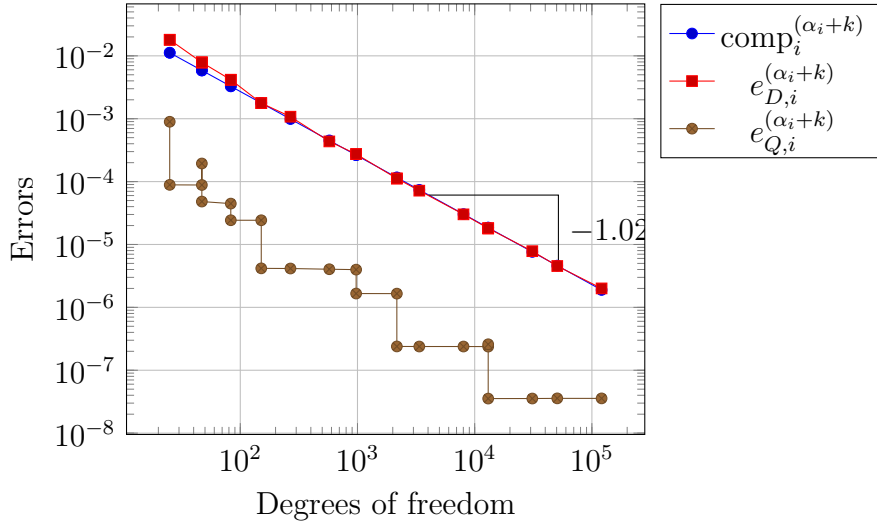


Figure 2: Quarter disk, linear problem: Decay of the computational error, the estimated discretization error and the estimated quadrature error.

DOF	$\text{comp}_i^{(\alpha_i+k)}$	$e_{D,i}^{(\alpha_i+k)}$	$e_{Q,i}^{(\alpha_i+k)}$	$\text{eff}^{(\alpha_i+k)}$	$\text{ind}_D^{(\alpha_i+k)}$
25	$1.803 \cdot 10^{-2}$	$8.875 \cdot 10^{-5}$	$1.801 \cdot 10^{-2}$	1.0036	1
47	$7.882 \cdot 10^{-3}$	$4.814 \cdot 10^{-5}$	$7.853 \cdot 10^{-3}$	1.0024	1
83	$4.127 \cdot 10^{-3}$	$2.429 \cdot 10^{-5}$	$4.164 \cdot 10^{-3}$	1.0149	1
151	$1.763 \cdot 10^{-3}$	$4.171 \cdot 10^{-6}$	$1.771 \cdot 10^{-3}$	1.0071	1
268	$1.072 \cdot 10^{-3}$	$4.148 \cdot 10^{-6}$	$1.077 \cdot 10^{-3}$	1.0088	1
575	$4.305 \cdot 10^{-4}$	$4.039 \cdot 10^{-6}$	$4.356 \cdot 10^{-4}$	1.0213	1
974	$2.762 \cdot 10^{-4}$	$1.659 \cdot 10^{-6}$	$2.739 \cdot 10^{-4}$	0.9978	1.00001
2167	$1.123 \cdot 10^{-4}$	$2.390 \cdot 10^{-7}$	$1.120 \cdot 10^{-4}$	0.9998	1.00001
3368	$7.205 \cdot 10^{-5}$	$2.384 \cdot 10^{-7}$	$7.176 \cdot 10^{-5}$	0.9992	1.00001
8026	$3.044 \cdot 10^{-5}$	$2.383 \cdot 10^{-7}$	$3.015 \cdot 10^{-5}$	0.9981	1.00001
13038	$1.802 \cdot 10^{-5}$	$3.542 \cdot 10^{-8}$	$1.806 \cdot 10^{-5}$	1.0037	1
31012	$7.793 \cdot 10^{-6}$	$3.549 \cdot 10^{-8}$	$7.825 \cdot 10^{-6}$	1.0086	1
50645	$4.511 \cdot 10^{-6}$	$3.570 \cdot 10^{-8}$	$4.542 \cdot 10^{-6}$	1.0149	1
120987	$1.970 \cdot 10^{-6}$	$3.566 \cdot 10^{-8}$	$2.001 \cdot 10^{-6}$	1.034	1.00001

Table 1: Quarter disk, linear problem: Number of degrees of freedom and associated computational error, estimated discretization and quadrature error, and effectivity and indicator indices.

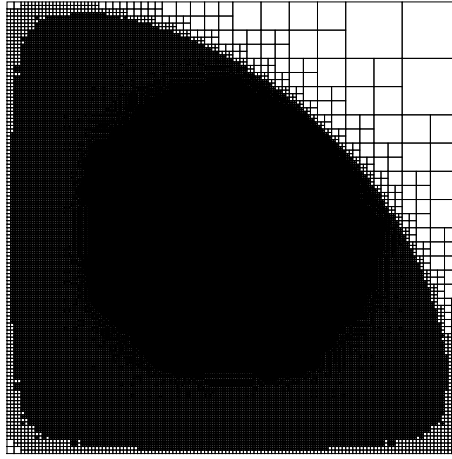


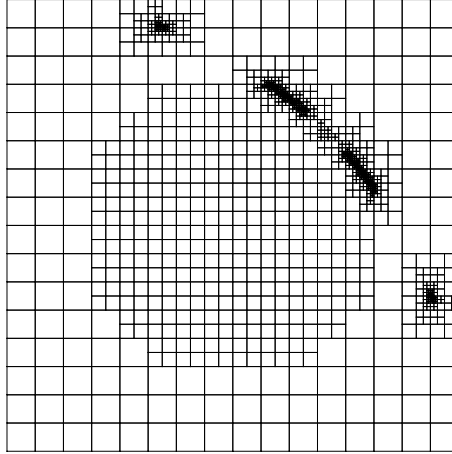
Figure 3: Quarter disk, linear problem: Final mesh with $\rho = 0.01$, approx. 120 000 DOF.

the localization nor taking the absolute value leads to a significant overestimation in this example.

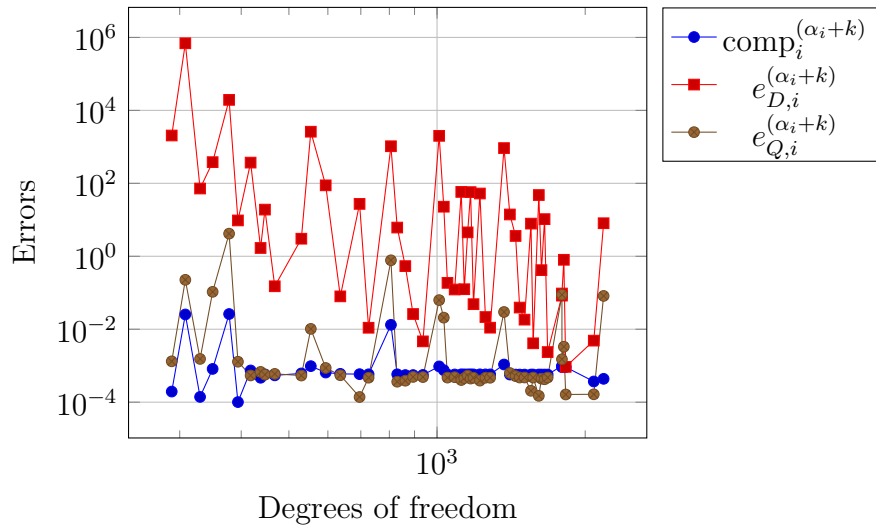
The error decays approximately as N^{-1} , which is the optimal algebraic convergence rate for this smooth problem when finite elements of polynomial degree 1 are used. We see that the quadrature mesh refinement step is carried out several times during the course of the refinement algorithm in order to reduce the quadrature error to a factor ρ of the discretization error. Also, it can be seen that the number of quadrature mesh refinements to reach a sufficient quadrature error reduction for a given finite-cell mesh lies between 0 and 2.

The final mesh with approx. 120 000 degrees of freedom is displayed in Figure 3. We see that the part of the unit square that does not lie within the unit disk is ignored by the finite-cell refinement. Also, the region near the circular boundary where the quadrature error is large is not refined in particular. This indicates that the separation of the discretization and the quadrature error portions performs well for this smooth problem.

Finally, we emphasize the dependence of the presented adaptive strategy on the parameter ρ used for balancing the error contributions. As usual, there is a tradeoff between accuracy and computational complexity, since choosing ρ smaller than necessary results in more quadrature mesh refinements, but is more likely to yield solutions of sufficient accuracy. Also, as outlined in Section 3, the accuracy of the error estimator in reflecting the true discretization error strongly depends on the accuracy of the discrete solution. For a demonstration of the effect when ρ is chosen too large, we use the setting from before with $\alpha_0 \equiv 2$, but change $\rho := 1.0$. The mesh resulting from 50 runs of the adaptive strategy is displayed in Figure 4a. We see that, instead of performing quadrature mesh refinements at the circular boundary, the strategy suggests finite-cell mesh refinements, yielding a mesh that is not suited to the problem. Also, the errors do not decay as expected, as can be seen in Figure 4b.



(a) Final mesh after 50 iterations, approx. 2000 DOF.



(b) Computational error, estimated discretization error and estimated quadrature error.

Figure 4: Quarter disk, linear problem with $\rho = 1.0$.

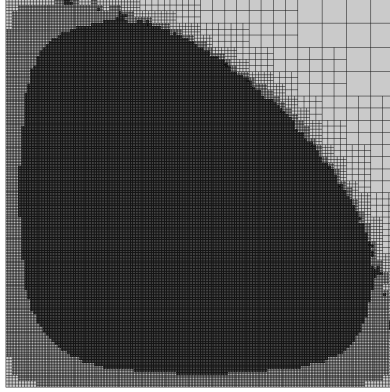


Figure 5: Quarter disk, nonlinear problem: Final mesh

5.1.2 Nonlinear problem

We solve the diffusion-reaction equation $-\Delta u + u^3 = f$, $u|_{\Gamma_D} = 0$, $\partial_n u|_{\Gamma_N} = g_N$ on the quarter disk. Its weak form reads

$$a(u)(v) = \int_{\Omega} \nabla u \cdot \nabla v + u^3 v = F(v) = \int_{\Omega} f v + \int_{\Gamma_N} g v$$

with Gateaux derivative

$$a'(u)(v, w) = \int_{\Omega} \nabla v \cdot \nabla w + 3u^2 v w.$$

As a goal functional, we choose $J(v) := \int_{\Omega} v$. The functions f and g_N are chosen such that the solution $u(x, y) := \sin(\pi x) \sin(\pi y)$ is obtained.

The approximations u^+ and z^+ are computed using patchwise biquadratic reconstruction as outlined in Section 3.1, see [2]. The error terms are localized to element-wise contributions with the filtering approach following Braack and Ern [9]. The estimates are transferred from nodes to the cells by calculating the mean over all estimates of nodes touching the cell. In this example, we use the optimal mesh strategy for marking, see [32]. The algorithmic parameters are set to $k := 3$ and $\rho := 0.01$.

Figure 5 shows the final mesh with approx. 180 000 DOF with a similar global refinement pattern as in the linear case. From Figure 6, we read the convergence rate of 1.0. Table 2 lists the numerical results corresponding to the finest quadrature mesh of each finite-cell mesh during the course of the refinement algorithm. The effectivity indices are close to 1.0, which implies that the estimation captures the true discretization error very well. From the indicator indices which lie between 1.3 and 1.9, we conclude that the localization using the filtering approach does not introduce significant overestimation.

In summary, the nonlinear problem displays behavior similar to the linear problem in terms of global mesh refinements and the optimal convergence rate.

5.2 Circular domain with reentrant corner

In a second series of experiments, we consider the circular domain with reentrant corner $\Omega := B_1(0) \setminus ([0, 1] \times [-1, 0])$. The Dirichlet boundary part is $\Gamma_D := ([0, 1] \times \{0\}) \cup (\{0\} \times$

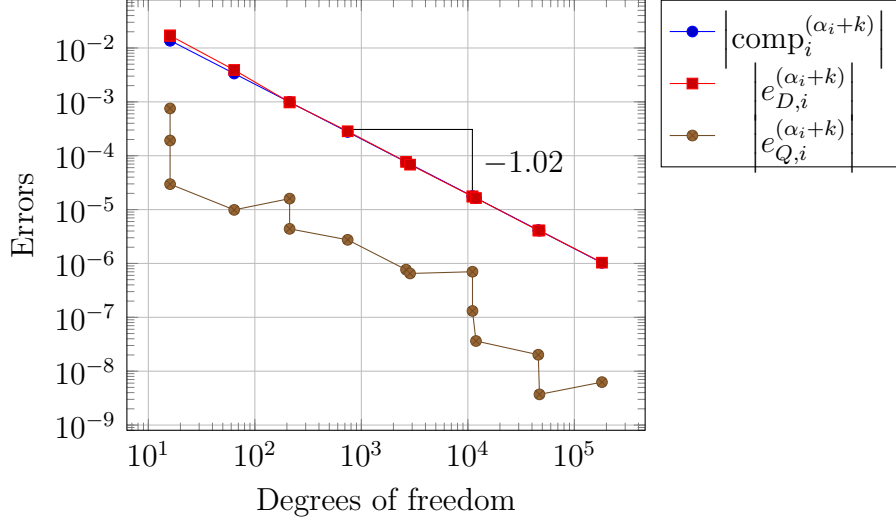


Figure 6: Quarter disk, nonlinear problem: Decay of the computational error, the estimated discretization error and the estimated quadrature error.

DOF	$ \text{comp}_i^{(\alpha_i+k)} $	$ e_{D,i}^{(\alpha_i+k)} $	$ e_{Q,i}^{(\alpha_i+k)} $	$\text{eff}^{(\alpha_i+k)}$	$\text{ind}_D^{(\alpha_i+k)}$
16	$1.545 \cdot 10^{-2}$	$1.698 \cdot 10^{-2}$	$2.965 \cdot 10^{-5}$	1.1009	1.3285
64	$3.875 \cdot 10^{-3}$	$3.908 \cdot 10^{-3}$	$9.873 \cdot 10^{-6}$	1.0059	1.628
212	$1.062 \cdot 10^{-3}$	$9.791 \cdot 10^{-4}$	$4.389 \cdot 10^{-6}$	0.9177	1.6951
744	$3.002 \cdot 10^{-4}$	$2.843 \cdot 10^{-4}$	$2.745 \cdot 10^{-6}$	0.9561	1.6463
2 628	$7.912 \cdot 10^{-5}$	$7.690 \cdot 10^{-5}$	$7.667 \cdot 10^{-7}$	0.9623	1.7619
2 868	$6.902 \cdot 10^{-5}$	$6.826 \cdot 10^{-5}$	$6.517 \cdot 10^{-7}$	0.9796	1.7255
11 052	$1.760 \cdot 10^{-5}$	$1.749 \cdot 10^{-5}$	$1.312 \cdot 10^{-7}$	0.9863	1.849
11 920	$1.647 \cdot 10^{-5}$	$1.638 \cdot 10^{-5}$	$3.634 \cdot 10^{-8}$	0.9966	1.7431
45 856	$4.165 \cdot 10^{-6}$	$4.081 \cdot 10^{-6}$	$2.020 \cdot 10^{-8}$	0.9848	1.8978
47 028	$4.102 \cdot 10^{-6}$	$4.102 \cdot 10^{-6}$	$3.710 \cdot 10^{-9}$	1.0009	1.7774
181 628	$1.029 \cdot 10^{-6}$	$1.034 \cdot 10^{-6}$	$6.268 \cdot 10^{-9}$	0.9986	1.8907

Table 2: Quarter disk, nonlinear problem: Number of degrees of freedom and associated computational error, estimated discretization and quadrature error, and effectivity and indicator indices.

$[-1, 0]$) and the Neumann boundary part is $\Gamma_N := \partial\Omega \setminus \Gamma_D$. For the discretization via the finite-cell method, we embed Ω into the L-shaped domain $\hat{\Omega} := (-1, 1)^2 \setminus ([0, 1] \times [-1, 0])$. The initial finite-cell mesh \mathcal{T}_0 consists of $3 \cdot 16$ square elements of order $p = 1$ and the initial depth α_0 is set to 2.

5.2.1 Linear problem

As a linear model problem where the solution has low regularity properties, we choose the Poisson problem $-\Delta u = 0$, $u|_{\Gamma_D} = 0$, $\partial_n u|_{\Gamma_N} = g_N$ on the domain Ω . The function g_N is chosen such that $u(r, \varphi) = r^{2/3} \sin(\frac{2}{3}\varphi)$ is the solution given in polar coordinates. Except for the circular arc on the Neumann boundary, this problem closely resembles the classical L-shaped domain problem. In particular, it features a corner singularity in $(0, 0)$. We choose $J(v) := \int_S v$ as a goal functional, where $S := [1/4, 1/2] \times [1/4, 1/2]$ is a subset of the domain. The corresponding dual problem in weak form is: Find $z \in H_{\Gamma_D}^1(\Omega)$ such that $\int_{\Omega} \nabla z \cdot \nabla \varphi = \int_S \varphi$ for all $\varphi \in H_{\Gamma_D}^1(\Omega)$.

As in Section 5.1.1, the exact solutions u, z are approximated by a higher-order finite-element solutions for which the same mesh \mathcal{T}_i , but finite elements of order $p = 2$ are used. The error estimates $e_{D,i}^{(\alpha_i+k)}$ and $e_{Q,i}^{(\alpha_i+k)}$ as well as the indicators for the discretization error $\eta_{D,T,i}^{(\alpha_i+k)}$ are computed with $k := 3$.

Since the exact solution u is known and the functional J can be evaluated up to machine precision on S , we compute $J(u) = \int_S u \approx 0.02047405612656314$.

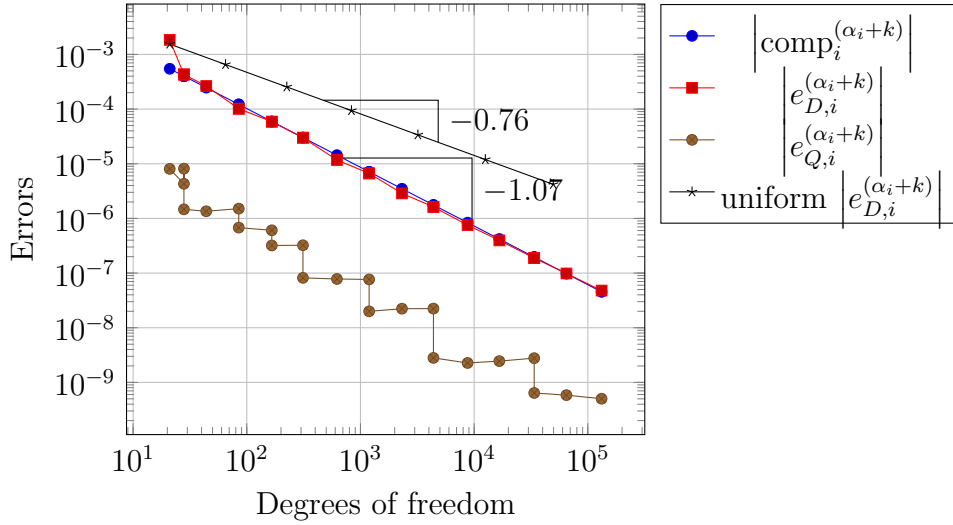


Figure 7: Reentrant corner domain, linear problem: Decay of the computational error, the estimated discretization error and the estimated quadrature error.

In Figure 7, the error terms from Equation (10) are displayed, visualizing the decay of the computational error $\text{comp}^{(\alpha_i+k)}$, the estimated discretization error $e_{D,i}^{(\alpha_i+k)}$, and the estimated quadrature error $e_{Q,i}^{(\alpha_i+k)}$. The error decays approximately as N^{-1} , which matches the optimal algebraic convergence rate for this problem using finite elements of polynomial degree 1. It can be seen that the adaptive strategy yields a convergence rate superior to the one delivered by the uniform refinement strategy, where the error decays approximately as $N^{-3/4}$.

DOF	$ \text{comp}_i^{(\alpha_i+k)} $	$ e_{D,i}^{(\alpha_i+k)} $	$ e_{Q,i}^{(\alpha_i+k)} $	$\text{eff}^{(\alpha_i+k)}$	$\text{ind}_D^{(\alpha_i+k)}$
21	$1.587 \cdot 10^{-2}$	$1.843 \cdot 10^{-3}$	$8.057 \cdot 10^{-6}$	0.1166	1.16846
28	$5.240 \cdot 10^{-4}$	$4.293 \cdot 10^{-4}$	$1.466 \cdot 10^{-6}$	0.8221	1.20719
44	$2.981 \cdot 10^{-4}$	$2.641 \cdot 10^{-4}$	$1.351 \cdot 10^{-6}$	0.8907	1.17441
85	$1.153 \cdot 10^{-4}$	$1.015 \cdot 10^{-4}$	$6.787 \cdot 10^{-7}$	0.8865	1.50728
166	$6.396 \cdot 10^{-5}$	$5.885 \cdot 10^{-5}$	$3.198 \cdot 10^{-7}$	0.9252	1.44238
312	$3.226 \cdot 10^{-5}$	$2.996 \cdot 10^{-5}$	$8.177 \cdot 10^{-8}$	0.9312	1.38439
621	$1.266 \cdot 10^{-5}$	$1.170 \cdot 10^{-5}$	$7.798 \cdot 10^{-8}$	0.9307	1.67064
1 192	$7.029 \cdot 10^{-6}$	$6.666 \cdot 10^{-6}$	$1.996 \cdot 10^{-8}$	0.9511	1.4689
2 318	$3.028 \cdot 10^{-6}$	$2.868 \cdot 10^{-6}$	$2.230 \cdot 10^{-8}$	0.9546	1.66408
4 385	$1.677 \cdot 10^{-6}$	$1.622 \cdot 10^{-6}$	$2.808 \cdot 10^{-9}$	0.9694	1.54452
8 757	$7.775 \cdot 10^{-7}$	$7.555 \cdot 10^{-7}$	$2.268 \cdot 10^{-9}$	0.9746	1.62021
16 648	$4.051 \cdot 10^{-7}$	$3.960 \cdot 10^{-7}$	$2.452 \cdot 10^{-9}$	0.9835	1.58728
33 749	$1.956 \cdot 10^{-7}$	$1.881 \cdot 10^{-7}$	$6.407 \cdot 10^{-10}$	0.9651	1.63535
64 833	$1.038 \cdot 10^{-7}$	$9.835 \cdot 10^{-8}$	$5.849 \cdot 10^{-10}$	0.9532	1.60085
132 180	$5.250 \cdot 10^{-8}$	$4.789 \cdot 10^{-8}$	$5.031 \cdot 10^{-10}$	0.9217	1.60678

Table 3: Reentrant corner domain, linear problem: Number of degrees of freedom and associated computational error, estimated discretization and quadrature error, and effectivity and indicator indices.

The numerical values corresponding to the finest quadrature mesh used for a given finite-cell mesh are displayed in Table 3. The effectivity indices are approximately 0.9, indicating that the exact error is mirrored by the estimation. The indicator indices lie between 1.0 and 2.0, which shows that the localization as well as the use of the absolute value introduce minor overestimation in this low-regularity example.

According to Figure 7, the quadrature mesh refinement step is performed several times to keep the quadrature error below a factor ρ of the discretization error. Again, the number of quadrature mesh refinements to reach a sufficient quadrature error reduction for a given finite-cell mesh lies between 0 and 2.

In contrast to the smooth problem, the domain features a corner singularity, which ought to be resolved by the adaptive algorithm. Indeed, upon inspection of the final mesh with approx. 130 000 degrees of freedom in Fig. 8, we see strong refinement around the corner singularity in $(0, 0)$. Also, the corners of the subdomain S are resolved by adaptive refinements. Additionally, the circular line with large quadrature error is ignored by the adaptive refinements which suggests that the separation of the discretization and the quadrature error works for this problem even though its solution has low regularity properties.

5.2.2 Nonlinear problem

As a nonlinear model problem, we solve the diffusion-reaction equation $-\Delta u + u^3 = f$, $u|_{\Gamma_D} = 0$, $\partial_n u|_{\Gamma_N} = g_N$. We choose $J(v) := \int_S v$ as the functional of interest. The approximation of u^+ , z^+ , the localization procedure as well as the choice of parameters are as described for the nonlinear problem in Section 5.1.2.

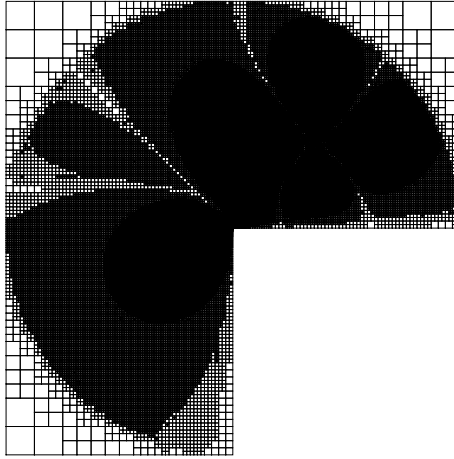


Figure 8: Reentrant corner domain, linear problem: Final mesh with approx. 130 000 DOF.

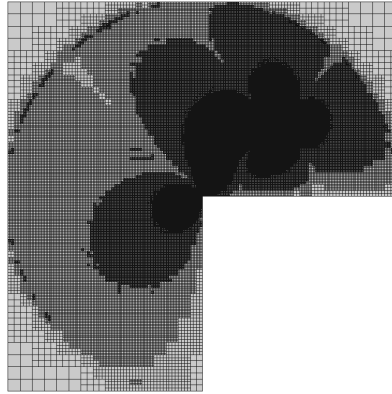


Figure 9: Reentrant corner domain, nonlinear problem: Final mesh with approx. 190 000 DOF.

As in the linear case, the optimal convergence rate of approximately 1.0 is attained, see Figure 10. In the mesh displayed in Figure 9, a moderate refinement of the finite-cell mesh towards the circular boundary can be seen, which, however, has no serious effect on the convergence rate. The corner singularity in $(0, 0)$ as well as the subdomain S are resolved by refinements. Finally, the numerical results are shown in Table 4 which demonstrate effectivity indices between 0.5 and 0.9 and moderate indicator indices between 1.3 and 2.6.

6 Conclusion

In this article, we presented a dual weighted residual (DWR) error estimator for the finite cell method (FCM). The DWR method allows for goal-oriented error control and incorporates the information of a user-defined goal functional into the solution of a dual problem that has to be solved alongside the primal problem. Since the FCM replaces the computational domain by a simpler enclosing domain on which the finite-element

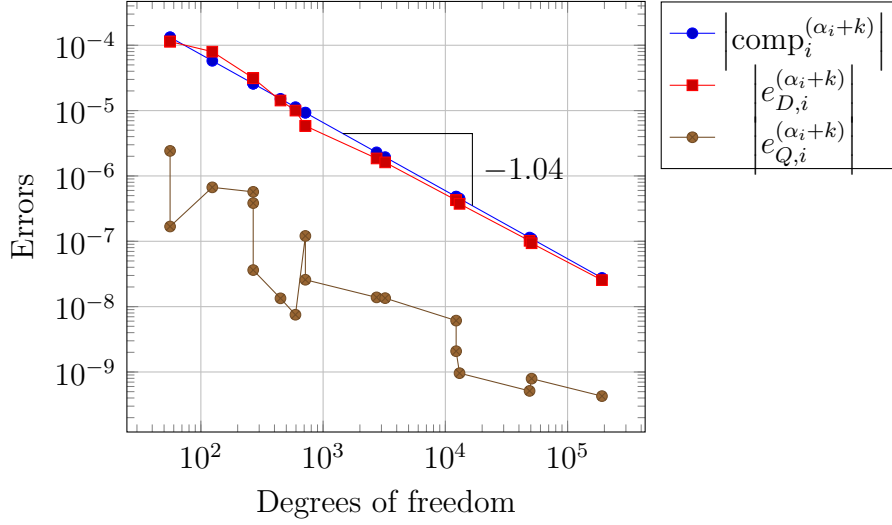


Figure 10: Reentrant corner domain, nonlinear problem: Decay of the computational error, the estimated discretization error and the estimated quadrature error.

DOF	$ \text{comp}_i^{(\alpha_i+k)} $	$ e_{D,i}^{(\alpha_i+k)} $	$ e_{Q,i}^{(\alpha_i+k)} $	$\text{eff}^{(\alpha_i+k)}$	$\text{ind}_D^{(\alpha_i+k)}$
56	$3.812 \cdot 10^{-4}$	$1.138 \cdot 10^{-4}$	$1.684 \cdot 10^{-7}$	0.2982	2.5422
124	$1.406 \cdot 10^{-4}$	$7.977 \cdot 10^{-5}$	$6.690 \cdot 10^{-7}$	0.5625	1.495
268	$5.586 \cdot 10^{-5}$	$3.127 \cdot 10^{-5}$	$3.628 \cdot 10^{-8}$	0.5591	1.3597
448	$2.437 \cdot 10^{-5}$	$1.426 \cdot 10^{-5}$	$1.340 \cdot 10^{-8}$	0.5846	1.3718
594	$1.444 \cdot 10^{-5}$	$1.000 \cdot 10^{-5}$	$7.520 \cdot 10^{-9}$	0.692	1.3018
716	$7.856 \cdot 10^{-6}$	$5.837 \cdot 10^{-6}$	$2.579 \cdot 10^{-8}$	0.7398	1.7867
2 738	$2.475 \cdot 10^{-6}$	$1.853 \cdot 10^{-6}$	$1.385 \cdot 10^{-8}$	0.7543	1.8462
3 218	$1.873 \cdot 10^{-6}$	$1.613 \cdot 10^{-6}$	$1.349 \cdot 10^{-8}$	0.8686	1.6411
12 254	$5.281 \cdot 10^{-7}$	$4.260 \cdot 10^{-7}$	$2.080 \cdot 10^{-9}$	0.8105	1.9135
13 064	$4.102 \cdot 10^{-7}$	$3.744 \cdot 10^{-7}$	$9.591 \cdot 10^{-10}$	0.915	1.8703
48 870	$1.168 \cdot 10^{-7}$	$1.017 \cdot 10^{-7}$	$5.133 \cdot 10^{-10}$	0.8753	2.0458
50 760	$9.959 \cdot 10^{-8}$	$9.336 \cdot 10^{-8}$	$7.906 \cdot 10^{-10}$	0.9453	1.9669
191 088	$2.767 \cdot 10^{-8}$	$2.545 \cdot 10^{-8}$	$4.272 \cdot 10^{-10}$	0.9353	2.231

Table 4: Reentrant corner domain, nonlinear problem: Number of degrees of freedom and associated computational error, estimated discretization and quadrature error, and effectivity and indicator indices.

space is constructed, the original, possibly complicated domain has to be approximated by a quadrature mesh. Thereby, a quadrature error is introduced. The presented method allows for splitting the DWR error contribution into an error term related to the discretization and an error term related to the quadrature. We suggested an adaptive strategy that refines the finite-cell or the quadrature mesh to balance the two error contributions. The effectivity of the strategy was underlined by linear and nonlinear numerical examples in 2D with smooth and low-regularity solutions.

References

- [1] Alireza Abedian, Jamshid Parvizian, Alexander Düster, and Ernst Rank. Finite cell method compared to h-version finite element method for elasto-plastic problems. *Applied Mathematics and Mechanics*, 35(10):1239–1248, 2014.
- [2] Wolfgang Bangerth and Rolf Rannacher. *Adaptive finite element methods for differential equations*. Birkhäuser, 2013.
- [3] R Becker, V Heuveline, and R Rannacher. An optimal control approach to adaptivity in computational fluid mechanics. *International journal for numerical methods in fluids*, 40(1-2):105–120, 2002.
- [4] Roland Becker, Claes Johnson, and Rolf Rannacher. Adaptive error control for multigrid finite element. *Computing*, 55(4):271–288, 1995.
- [5] Roland Becker and Rolf Rannacher. An optimal control approach to a posteriori error estimation in finite element methods. *Acta Numerica 2001*, 10:1–102, 2001.
- [6] H. Blum, A. Schröder, and F. T. Suttmeier. *A posteriori estimates for FE-solutions of variational inequalities*, pages 669–680. Springer Milan, Milano, 2003.
- [7] Heribert Blum and F-T Suttmeier. An adaptive finite element discretisation for a simplified signorini problem. *Calcolo*, 37(2):65–77, 2000.
- [8] Malte Braack and Alexandre Ern. Adaptive computation of reactive flows with local mesh refinement and model adaptation. In *Numerical mathematics and advanced applications*, pages 159–168. Springer, 2004.
- [9] Malte Braack and Alexandre Ern. Coupling multimodelling with local mesh refinement for the numerical computation of laminar flames. *Combustion Theory and Modelling*, 8(4):771–788, 2004.
- [10] Dietrich Braess. *Finite Elemente: Theorie, schnelle Löser und Anwendungen in der Elastizitätstheorie*. Springer-Verlag, 2013.
- [11] Monique Dauge, Alexander Düster, and Ernst Rank. Theoretical and numerical investigation of the finite cell method. *Journal of Scientific Computing*, 65(3):1039–1064, 2015.
- [12] Mark De Berg, Marc Van Kreveld, Mark Overmars, and Otfried Cheong Schwarzkopf. *Computational Geometry*. Springer, 2000.

-
- [13] Willy Dörfler. A convergent adaptive algorithm for poisson’s equation. *SIAM Journal on Numerical Analysis*, 33(3):1106–1124, 1996.
- [14] Alexander Düster, Jamshid Parvizian, Zhengxiong Yang, and Ernst Rank. The finite cell method for three-dimensional problems of solid mechanics. *Computer methods in applied mechanics and engineering*, 197(45):3768–3782, 2008.
- [15] Kenneth Eriksson, Don Estep, Peter Hansbo, and Claes Johnson. Introduction to adaptive methods for differential equations. *Acta numerica*, 4:105–158, 1995.
- [16] R Glowinski and Yu Kuznetsov. Distributed lagrange multipliers based on fictitious domain method for second order elliptic problems. *Computer Methods in Applied Mechanics and Engineering*, 196(8):1498–1506, 2007.
- [17] Roland Glowinski, Tsorng-Whay Pan, and Jacques Periaux. A fictitious domain method for dirichlet problem and applications. *Computer Methods in Applied Mechanics and Engineering*, 111(3-4):283–303, 1994.
- [18] Thomas Grätsch and Klaus-Jürgen Bathe. Goal-oriented error estimation in the analysis of fluid flows with structural interactions. *Computer methods in applied mechanics and engineering*, 195(41):5673–5684, 2006.
- [19] Meysam Joulaian, Sascha Duczak, Ulrich Gabbert, and Alexander Düster. Finite and spectral cell method for wave propagation in heterogeneous materials. *Computational Mechanics*, 54(3):661–675, 2014.
- [20] Meysam Joulaian, Simeon Hubrich, and Alexander Düster. Numerical integration of discontinuities on arbitrary domains based on moment fitting. *Computational Mechanics*, 57(6):979–999, 2016.
- [21] László Kudela, Nils Zander, Tino Bog, Stefan Kollmannsberger, and Ernst Rank. Efficient and accurate numerical quadrature for immersed boundary methods. *Advanced Modeling and Simulation in Engineering Sciences*, 2(1):10, 2015.
- [22] László Kudela, Nils Zander, Stefan Kollmannsberger, and Ernst Rank. Smart octrees: Accurately integrating discontinuous functions in 3d. *Computer Methods in Applied Mechanics and Engineering*, 306:406–426, 2016.
- [23] J. Nitsche. Über ein variationsprinzip zur lösung von dirichlet-problemen bei verwendung von teilräumen, die keinen randbedingungen unterworfen sind. *Abhandlungen aus dem Mathematischen Seminar der Universität Hamburg*, 36(1):9–15, 1971.
- [24] Marius Paraschivoiu, Jaime Peraire, and Anthony T Patera. A posteriori finite element bounds for linear-functional outputs of elliptic partial differential equations. *Computer methods in applied mechanics and engineering*, 150(1-4):289–312, 1997.
- [25] J Parvizian, A Düster, and E Rank. Topology optimization using the finite cell method. *Optimization and Engineering*, 13(1):57–78, 2012.
- [26] Jamshid Parvizian, Alexander Düster, and Ernst Rank. Finite cell method. *Computational Mechanics*, 41(1):121–133, 2007.

-
- [27] Serge Prudhomme and J Tinsley Oden. On goal-oriented error estimation for elliptic problems: application to the control of pointwise errors. *Computer Methods in Applied Mechanics and Engineering*, 176(1-4):313–331, 1999.
- [28] Andreas Rademacher. *Adaptive finite element methods for nonlinear hyperbolic problems of second order*. PhD thesis, TU Dortmund, 2010.
- [29] Andreas Rademacher and Andreas Schröder. Dual weighted residual error control for frictional contact problems. *Comput. Meth. in Appl. Math.*, 15(3):391–413, 2015.
- [30] Ernst Rank, Stefan Kollmannsberger, Ch Sorger, and Alexander Düster. Shell finite cell method: a high order fictitious domain approach for thin-walled structures. *Computer Methods in Applied Mechanics and Engineering*, 200(45):3200–3209, 2011.
- [31] Rolf Rannacher and Jevgeni Vihharev. Adaptive finite element analysis of nonlinear problems: balancing of discretization and iteration errors. *Journal of Numerical Mathematics*, 21(1):23–62, 2013.
- [32] T. Richter. *Parallel multigrid method for adaptive finite elements with application to 3D flow problems*. PhD thesis, Ruprecht-Karls-Universität Heidelberg, 2005.
- [33] Th Richter. Goal-oriented error estimation for fluid–structure interaction problems. *Computer Methods in Applied Mechanics and Engineering*, 223:28–42, 2012.
- [34] Thomas Richter and Thomas Wick. Variational localizations of the dual weighted residual estimator. *Journal of Computational and Applied Mathematics*, 279:192–208, 2015.
- [35] Valerij K Saul’ev. On the solution of some boundary value problems on high performance computers by fictitious domain method. *Siberian Math. J*, 4(4):912–925, 1963.
- [36] A Schröder and A Rademacher. Goal-oriented error control in adaptive mixed fem for signorini’s problem. *Computer Methods in Applied Mechanics and Engineering*, 200(1):345–355, 2011.
- [37] Kristoffer G van der Zee, E Harald van Brummelen, Ido Akkerman, and René de Borst. Goal-oriented error estimation and adaptivity for fluid–structure interaction using exact linearized adjoints. *Computer Methods in Applied Mechanics and Engineering*, 200(37):2738–2757, 2011.
- [38] Thomas Wick. Goal-oriented mesh adaptivity for fluid-structure interaction with application to heart-valve settings. *Archive of Mechanical Engineering*, 59(1):73–99, 2012.
- [39] Z Yang, M Ruess, S Kollmannsberger, A Düster, and E Rank. An efficient integration technique for the voxel-based finite cell method. *International Journal for Numerical Methods in Engineering*, 91(5):457–471, 2012.

-
- [40] Zhengxiong Yang, Stefan Kollmannsberger, Alexander Düster, Martin Ruess, Eduardo Grande Garcia, Rainer Burgkart, and Ernst Rank. Non-standard bone simulation: interactive numerical analysis by computational steering. *Computing and Visualization in Science*, 14(5):207–216, 2011.
- [41] N. Zander, T. Bog, M. Elhaddad, R. Espinoza, H. Hu, A. Joly, C. Wu, P. Zerbe, A. Düster, S. Kollmannsberger, J. Parvizian, M. Ruess, D. Schillinger, and E. Rank. Fcmlab: A finite cell research toolbox for {MATLAB}. *Advances in Engineering Software*, 74:49 – 63, 2014.